cosmetics

MDPI

Article

Transcriptomic Effects of *Pinus densiflora* Needle Extract on Human Hair Follicle Dermal Papilla Cells: Estrogen- and Sterol-Related Signaling

Hisako Iwahashi Ogawa [1,2], Aprill Kee Oliva Mizushima [3], Farhana Ferdousi [1,3,4,5], Mitsutoshi Nakajima [3,6] and Hiroko Isoda [1,3,4,5,6,7,*]

1 Graduate School of Science and Technology, University of Tsukuba, Tsukuba 305-8572, Ibaraki, Japan
2 Arakawa Chemical Industries, Ltd., 1-3-7, Hiranomachi, Chuo-ku, Osaka 541-0046, Japan
3 Alliance for Research on the Mediterranean and North Africa, University of Tsukuba, Tsukuba 305-8572, Ibaraki, Japan
4 Institute of Life and Environmental Sciences, University of Tsukuba, 1-1-1 Tennodai, Tsukuba 305-8575, Ibaraki, Japan
5 Tsukuba Life Science Innovation Program (T-LSI), University of Tsukuba, Tsukuba 305-8572, Ibaraki, Japan
6 MED R&D Co., Ltd., Tsukuba 305-8572, Ibaraki, Japan
7 Open Innovation Laboratory for Food and Medicinal Resource Engineering (FoodMed-OIL), National Institute of Advanced Industrial Science and Technology (AIST), Tsukuba 305-0821, Ibaraki, Japan
* Correspondence: isoda.hiroko.ga@u.tsukuba.ac.jp

Abstract

Pinus densiflora needle extract (PN) contains multiple constituents and has previously shown biological activities relevant to stress- and hormone-associated signaling; however, its molecular effects in human hair follicle dermal papilla cells (HFDPCs) remain incompletely understood. This study investigated PN-induced transcriptional responses in HFDPCs, with particular focus on follicle-related, estrogen-related, and sterol biosynthesis-associated pathways. Cell viability and the expression of *ALPL*, *CTNNB1*, and *FGF1* were evaluated following treatment with PN and selected PN-derived components, while *ESR1* expression was examined separately following PN treatment. Whole-genome microarray analysis was combined with pathway, protein–protein interaction, and gene set enrichment analyses, together with molecular docking targeting estrogen receptor alpha (ERα). PN did not markedly reduce HFDPC viability and significantly increased *ALPL*, *CTNNB1*, and *FGF1* expression. Several PN-derived components partially reproduced these responses, whereas a five-compound mixture reproduced a broader range of the extract-associated gene expression changes. Transcriptomic analyses identified pathways related to growth regulation, Wnt, estrogen signaling, and steroid biosynthesis. Gene set enrichment analysis further identified significant enrichment of steroid biosynthesis accompanied by coordinated changes in sterol biosynthesis-related genes. PN treatment also significantly increased *ESR1* expression as determined by RT-qPCR. PN-derived compounds showed weaker predicted ERα binding than 17β-estradiol, providing no evidence for strong direct interaction with ERα. Overall, PN induced coordinated transcriptional changes involving follicle-relevant, estrogen-related, and sterol biosynthesis-related pathways. Further functional studies are required because hair growth and sterol or hormone production were not directly measured.

Keywords: *Pinus densiflora*; estrogen signaling; hair growth; dermal papilla cells; transcriptomics; steroid biosynthesis

Academic Editor: Enzo Berardesca

Received: 13 October 2026
Revised: 4 November 2026
Accepted: 11 November 2026
Published: 23 November 2026

Copyright: © 2026 by the authors. Licensee MDPI, Basel, Switzerland. This article is an open access article distributed under the terms and conditions of the Creative Commons Attribution (CC BY) license.

1. Introduction

Hair loss, including alopecia, is a common condition that can substantially affect quality of life and psychosocial well-being in both men and women. In addition to cosmetic concerns, hair loss is frequently associated with reduced self-esteem, emotional distress, and impaired daily functioning [1,2]. Although minoxidil and finasteride are widely used for the management of hair loss, their efficacy is variable, and their use may be limited by adverse effects and poor long-term adherence [3,4]. These limitations have increased interest in plant-derived materials and natural products as sources of bioactive compounds relevant to hair and scalp research.

The hair follicle undergoes cyclic phases of growth (anagen), regression (catagen), and rest (telogen) [5]. Hair follicle activity is maintained by tightly regulated epithelial–mesenchymal interactions within the follicular niche, particularly those involving dermal papilla cells. Human hair follicle dermal papilla cells (HFDPCs) play a central role in coordinating follicular signaling and anagen-associated activity and are therefore widely used as an experimental model for studying molecular processes relevant to hair follicle biology. Among the signaling pathways involved, Wnt/β-catenin signaling is a key regulator of hair follicle development and cycling [6], while fibroblast growth factor signaling contributes to follicular growth regulation [7]. Alkaline phosphatase activity is also associated with dermal papilla characteristics and hair-cycle regulation [8]. Accordingly, *CTNNB1*, *FGF1*, and *ALPL* were selected in the present study as representative follicle-related genes reflecting these biological processes.

Pinus densiflora Siebold & Zucc. (Japanese red pine) is widely distributed in East Asia and has a long history of traditional use. Pine needles have long been consumed as a traditional health-promoting medicinal food in Korea [9], and various parts of *P. densiflora*, including the needles, are described in classical East Asian pharmacopeias such as the Chinese *Compendium of Materia Medica* (*Bencao Gangmu*) [10]. In addition, pine needle preparations have been reported to exhibit several biological activities, including antioxidant, antiviral, and antithrombotic effects [9–11]. We previously reported that a hot-water extract of *P. densiflora* needles exerted antidepressant-like and neuroprotective effects in a mouse model [12]. Chemical analysis of the same extract identified several low-molecular-weight constituents, including D-pinitol, shikimic acid, catechol, hydroquinone, and 3-hydroxybenzoic acid [12]. This history of traditional use, together with the reported biological activities of *P. densiflora* needle preparations, provided a rationale for investigating the molecular effects of *P. densiflora* needle extract (PN) in HFDPCs.

Estrogen-related signaling is also relevant to hair follicle physiology, although its effects are dependent on receptor subtype, follicular compartment, and hormonal context. Human hair follicles can act as both targets and local sources of estrogen-related signaling, and classical estrogen receptors are expressed in multiple follicular compartments [13]. In dermal papilla cells, estrogen-related signaling can influence cellular activity through both nuclear estrogen receptors and membrane-associated receptors. Recent studies have provided additional mechanistic evidence for these effects. Activation of the G protein-coupled estrogen receptor GPR30/GPER in human dermal papilla cells enhanced Wnt/Hedgehog signaling, pathways associated with follicular activity [14]. In addition, ERα-associated signaling in cultured human dermal papilla cells has been linked to MAPK-associated signaling, growth-factor expression, cellular proliferation, and mitochondrial activity [15]. These observations indicate that estrogen-responsive pathways may modulate dermal papilla cell function through multiple interconnected signaling mechanisms rather than through a single pathway. Together with the established importance of Wnt/β-catenin signaling in follicle biology, this provides a mechanistic basis for examining estrogen-related transcriptional responses to PN in HFDPCs.

https://doi.org/10.3390/cosmetics13060331

In the present study, we evaluated the effects of PN on HFDPC viability, selected follicle-related gene expression, and whole-transcriptome responses. We further examined major PN-derived components and investigated estrogen- and sterol biosynthesis-related transcriptional features using microarray-based pathway analysis, protein–protein interaction network analysis, gene set enrichment analysis, *ESR1* expression analysis, and molecular docking. In addition, an exploratory comparative transcriptomic analysis integrating HFDPC and mouse hippocampal datasets was performed to examine whether hormone-related regulatory features were represented across these distinct biological contexts.

The ultimate objective of this study was to characterize the molecular response of HFDPCs to PN and to identify transcriptional pathways that may provide a basis for future functional investigation of PN in hair follicle biology.

2. Materials and Methods

2.1. Preparation of Hot-Water Extract of Pine Needles

The *Pinus densiflora* needle extract (PN) used in this study was prepared as described previously [12], with additional details provided here for reproducibility. *P. densiflora* needles were obtained from a commercial supplier in Okayama Prefecture, Japan, in April 2023. Species identification information was provided by the supplier, and the identity of the plant material was additionally confirmed by morphological assessment. Dried and crushed pine needles (1 g) were extracted with 10 mL of distilled water at 105 °C for 30 min using an autoclave. The resulting extract was filtered through a 0.2 μm membrane filter and used for subsequent biological assays. The total solid content of the PN stock extract was 2.1% (*w*/*w*), as determined gravimetrically by drying a 0.1 g aliquot of the extract and weighing the dried residue.

2.2. Chemical Characterization of the Hot-Water Extract of PN

The chemical composition of PN was previously characterized by gas chromatography–mass spectrometry (GC/MS) and high-performance liquid chromatography (HPLC) using authentic standards [12]. The major quantified constituents in the undiluted PN extract were D-pinitol (2376 ppm), shikimic acid (5930 ppm), catechol (200 ppm), hydroquinone (162 ppm), and 3-hydroxybenzoic acid (5 ppm). The same PN preparation was used in the present HFDPC experiments. PN treatment concentrations are expressed as dilution ratios of this chemically characterized stock extract.

2.3. Cell Culture and Treatment Conditions

Human hair follicle dermal papilla cells (HFDPCs) were purchased from PromoCell (Heidelberg, Germany; C-12071, Lot No. 485Z013). According to the manufacturer's certificate of analysis, the cells were derived from the temple skin of a 66-year-old female donor and supplied at passage 2. HFDPCs were maintained in Follicle Dermal Papilla Cell Growth Medium supplemented with fetal calf serum, insulin, transferrin, triiodothyronine, bovine pituitary extract, and cyproterone solution according to the manufacturer's instructions.

Cells were cultured in 75 cm^2 flasks at 37 °C in a humidified atmosphere containing 5% CO_2, and the medium was changed every 2 days. HFDPCs were passaged before reaching 80% confluence and used for experiments up to passage 6. Minoxidil, catechol, hydroquinone, 3-hydroxybenzoic acid, shikimic acid, and D-pinitol were purchased from Tokyo Chemical Industry Co., Ltd. (Tokyo, Japan).

For analysis of follicle-related gene expression, HFDPCs were treated for 48 h with PN at dilutions of 1/2000 and 1/500 or with 0.1 μM minoxidil as a positive control. The expression levels of *CTNNB1*, *ALPL*, and *FGF1* were then evaluated by RT-qPCR.

To examine the contribution of major PN-derived constituents, catechol was tested at 0.91 and 3.63 μM, hydroquinone at 0.74 and 2.94 μM, and 3-hydroxybenzoic acid at 0.018 and 0.072 μM. These concentrations corresponded to the amounts of the respective compounds present in PN at dilutions of 1/2000 and 1/500. In the individual-compound experiments, shikimic acid and D-pinitol were evaluated at fixed concentrations of 1 and 10 μM; these concentrations were not intended to represent PN-equivalent dilution conditions. In contrast, the five-component mixture containing D-pinitol, shikimic acid, catechol, hydroquinone, and 3-hydroxybenzoic acid was prepared so that all five constituents reproduced their respective concentrations in PN at dilutions of 1/2000 and 1/500 (Supplementary Table S1).

For analysis of *ESR1* expression, HFDPCs were treated with PN at a dilution of 1/2000 for 6, 12, or 24 h.

2.4. Cell Viability Assay

Cell viability was evaluated using the MTT assay. MTT was purchased from Dojindo Laboratories (Kumamoto, Japan). HFDPCs were seeded in collagen-coated 96-well plates at a density of 3×10^4 cells/well and incubated overnight to allow cell attachment. Cells were then treated with PN at dilutions of 1/100, 1/250, 1/500, 1/1000, 1/2000, 1/4000, and 1/6000 for 48 h.

The major PN-derived constituents—D-pinitol, shikimic acid, catechol, hydroquinone, and 3-hydroxybenzoic acid—were also evaluated individually and as a five-component mixture. Catechol, hydroquinone, and 3-hydroxybenzoic acid were tested over PN-equivalent concentration ranges corresponding to the PN dilution ratios shown in Figure 1B, whereas shikimic acid and D-pinitol were evaluated at fixed concentrations ranging from 0.05 to 100 μM. The five-component mixture was evaluated at PN-equivalent dilution ratios as indicated in Figure 1B.

After treatment, MTT solution was added to a final concentration of 5 mg/mL, and the cells were incubated for 4 h. Subsequently, 10% sodium dodecyl sulfate (SDS) solution was added, followed by overnight incubation. Absorbance was measured at 570 nm using a Varioskan LUX multimode microplate reader (Thermo Fisher Scientific, Waltham, MA, USA).

Cell viability was expressed as a percentage relative to untreated control cells.

2.5. RNA Extraction

HFDPCs were seeded in collagen-coated 6-well plates at a density of 3×10^4 cells/well and incubated overnight to allow attachment. After treatment under the conditions described in Section 2.3, total RNA was extracted using the ISOGEN kit (Nippon Gene, Tokyo, Japan) according to the manufacturer's instructions. RNA concentration and purity were assessed using a NanoDrop 2000 spectrophotometer (Thermo Fisher Scientific, Wilmington, DE, USA).

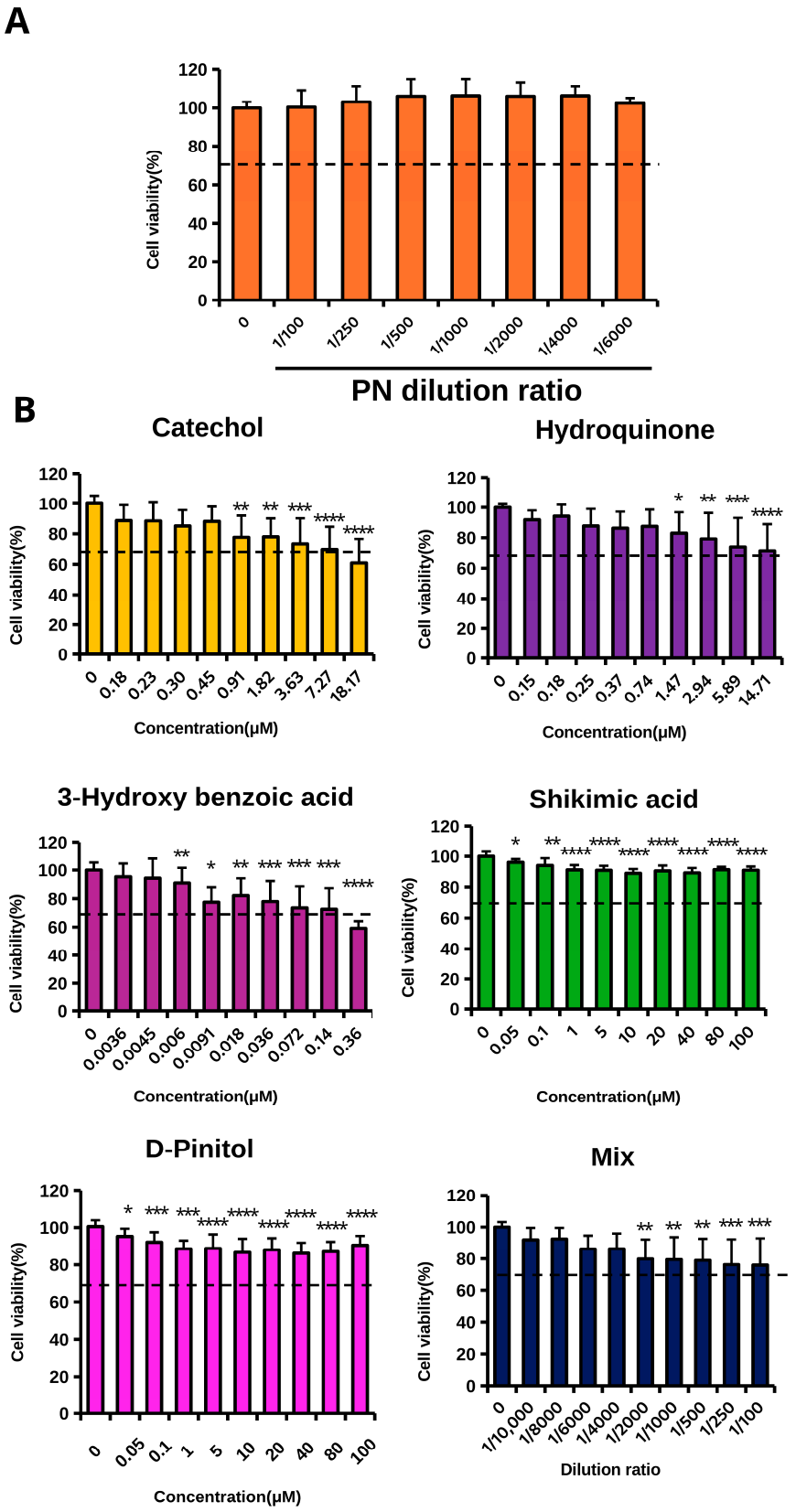

Figure 1. Effects of PN and PN-derived components on HFDPC viability. (**A**) HFDPCs were treated with the indicated PN dilution ratios for 48 h, and cell viability was assessed using the MTT assay. The dashed line indicates 70% viability as a practical reference threshold for concentration selection in subsequent experiments. (**B**) HFDPCs were treated for 48 h with the indicated concentrations of

catechol, hydroquinone, 3-hydroxybenzoic acid, shikimic acid, and D-pinitol, or with the five-component mixture at the indicated PN-equivalent dilution ratios, and cell viability was assessed using the MTT assay. Data are presented as mean ± SD from three independent experiments. Statistical significance was evaluated by one-way ANOVA followed by Dunnett's multiple-comparison test, with each treatment group compared with the untreated control. Only statistically significant differences are indicated: * $p < 0.05$, ** $p < 0.01$, *** $p < 0.001$, and **** $p < 0.0001$.

2.6. TaqMan RT-qPCR Analysis

Total RNA was reverse-transcribed into cDNA using SuperScript IV VILO Master Mix (Invitrogen, Thermo Fisher Scientific, Waltham, MA, USA) according to the manufacturer's instructions. RT-qPCR was performed using TaqMan Universal Master Mix and gene-specific TaqMan assays for *CTNNB1* (Hs00355045_m1), *ALPL* (Hs01029144_m1), *FGF1* (Hs01092738_m1), and *ESR1* (Hs01046816_m1) (Applied Biosystems, Thermo Fisher Scientific, Foster City, CA, USA).

Amplification and detection were performed using a 7500 Fast Real-Time PCR System operated with 7500 Fast Real-Time PCR Software version 1.3.1 (Applied Biosystems, Thermo Fisher Scientific, Foster City, CA, USA). *GAPDH* (Hs02786624_g1) was used as the endogenous reference gene. Relative gene expression was calculated using the $2^{-\Delta\Delta Ct}$ method. For each sample, ΔCt was calculated as Ct_target − Ct_GAPDH, and ΔΔCt was calculated relative to the corresponding untreated control group. Relative expression values were expressed as $2^{-\Delta\Delta Ct}$. Amplification reactions were performed in technical triplicate, and data shown in the figures represent three independent experiments.

2.7. Molecular Docking Analysis Targeting ERα

Molecular docking simulations were performed to assess predicted interactions between PN-derived compounds and estrogen receptor alpha (ERα). The crystal structure of ERα was obtained from the Protein Data Bank (PDB ID: 3ERD). Water molecules and co-crystallized ligands were removed, polar hydrogens were added, and the receptor was treated as rigid. Docking simulations were conducted using AutoDock Vina version 1.2.7. The grid box was centered at X = 1.36, Y = −4.19, and Z = 8.19, with dimensions of 22 × 22 × 22 Å and a grid spacing of 0.375 Å. The exhaustiveness parameter was set to 8. Predicted binding affinity was evaluated using the best docking score obtained for each ligand. Ionization states of the ligands were considered when relevant. Protein–ligand complexes were visualized using PyMOL Molecular Graphics System version 3.1.6.1 (Schrödinger, LLC, New York, NY, USA).

2.8. Microarray Analysis

Microarray analysis was performed using RNA samples from HFDPCs treated with PN at a dilution of 1/500. Three biological replicates were analyzed for each group. Gene expression profiling was conducted using the Clariom S Assay Human system (Thermo Fisher Scientific, Tokyo, Japan). cDNA was generated using the GeneChip WT Plus Reagent Kit (Thermo Fisher Scientific) according to the manufacturer's instructions. Samples were hybridized to Clariom S Human arrays, followed by washing and staining. Images were acquired using a GeneChip Scanner 3000 (Thermo Fisher Scientific), and raw signal intensity data were generated for subsequent analysis.

2.9. Transcriptomic Data Processing and Bioinformatic Analyses

Raw microarray data from HFDPCs were processed using Transcriptome Analysis Console (TAC) software version 4.0.2 (Thermo Fisher Scientific, Waltham, MA, USA). Signal intensities were normalized using the signal space transformation robust multi-array average (SST-RMA) algorithm implemented in TAC. Gene-level statistical analysis was

performed using the limma Bioconductor framework integrated within TAC. A detected above background (DABG) threshold of 0.05 was applied, and genes with positive-versus-negative area under the curve (AUC) values ≥ 0.7 were retained.

Genes satisfying these quality criteria were considered PN-responsive if they met both a p value threshold of < 0.05 and a signed fold change threshold of either > 1.1 or < −1.1. A total of 1336 PN-responsive genes, including 667 upregulated and 669 downregulated genes, were identified. For subsequent STRING-based PPI network analysis, the upregulated genes were further restricted using a fold-change cutoff of ≥1.4 to obtain a more focused set of PN-responsive genes for network-level analysis.

The volcano plot in Figure 3A was generated from the original TAC derived signed fold change and p value data using Python (version 3.13.5) and Matplotlib (version 3.10.8) [16].

Gene Ontology (GO) and Kyoto Encyclopedia of Genes and Genomes (KEGG) enrichment analyses were performed using the Metascape web platform (version 3.5.20240101; accessed 18 June 2025) [17].

Protein–protein interaction (PPI) network analysis was performed using NetworkAnalyst version 3.0 [18]. PPI network construction was based on curated interactome resources, including the IMEx Interactome database, which integrates interaction data from multiple resources such as InnateDB [19].

To further characterize PN-responsive signaling programs in HFDPCs, upregulated PN-responsive genes were additionally mapped to the STRING interactome using a first-order network option, a confidence score cutoff of 900, and experimental evidence enabled. KEGG pathway enrichment analysis was then performed on the resulting PPI-derived network. An estrogen-related subnetwork was subsequently extracted from this PN-responsive network to examine proteins associated with estrogen signaling.

GSEA was performed using the web-based ExpressAnalyst platform [20] (https://www.expressanalyst.ca/; accessed on 23 July 2025) with the SST-RMA-normalized expression matrix comprising three PN-treated and three control HFDPC samples.

No additional normalization was applied in ExpressAnalyst. Genes were ranked according to fold change, and KEGG pathway gene sets were used for enrichment analysis. For the steroid biosynthesis pathway identified by GSEA, the associated expression-pattern heatmap was generated directly in ExpressAnalyst using the pathway-mapped genes present in the analyzed expression dataset.

For exploratory comparative transcriptomic analysis, the HFDPC dataset generated in the present study was compared with a previously published mouse hippocampal microarray dataset obtained from PN-treated mice [12]. The hippocampal dataset is available in the NCBI Gene Expression Omnibus (GEO) under accession number GSE293650. Raw Affymetrix CEL files from the mouse hippocampal dataset were background-corrected, normalized, and summarized using the robust multichip average (RMA) algorithm implemented in TAC software version 4.0.1 [21].

Each dataset was processed using the web-based ExpressAnalyst platform [20] (https://www.expressanalyst.ca/; accessed on 20 August 2025), which uses the ExpressAnalystR package for back-end computations. The limma method was used to identify PN-responsive genes between treated and control groups.

Mouse gene symbols were converted to their human orthologs for annotation and enrichment analysis using the default criteria of the Metascape web tool. For the exploratory comparative analysis, genes with a linear fold change ≥1.1 or ≤−1.1 and $p < 0.05$ were retained as PN-responsive genes for subsequent network-level analysis. This relatively permissive threshold was used to capture modest PN-associated expression changes across datasets differing in species, tissue type, microarray platform, and experimental

conditions. This criterion was used for hypothesis-generating analysis and was not intended to define a conventional set of differentially expressed genes.

PN-responsive genes derived from the HFDPC and mouse hippocampal datasets were integrated and subjected to pathway-oriented network analysis using NetworkAnalyst. A zero-order PPI network was constructed to retain direct interactions among input genes without introducing intermediate connector nodes. KEGG-based functional exploration of the resulting comparative PPI network was performed using the Function Explorer module in NetworkAnalyst. Genes assigned to the KEGG oocyte meiosis pathway were extracted to define an oocyte meiosis-associated subnetwork, which was subsequently subjected to additional KEGG enrichment analysis.

2.10. Statistical Analysis

Statistical analyses were performed using GraphPad Prism version 10 (GraphPad Software Inc., San Diego, CA, USA). Data are presented as mean ± standard deviation (SD) unless otherwise stated. Normality was assessed using the Shapiro–Wilk test. For comparisons between two groups, an unpaired Student's *t*-test was used. For comparisons among multiple groups, one-way analysis of variance (ANOVA) followed by Dunnett's post hoc test was used. Differences were considered statistically significant at $p < 0.05$.

2.11. Use of Artificial Intelligence-Assisted Language Editing

Satellite AI was used solely for English-language polishing of the manuscript. It was not used to generate experimental data, perform statistical analyses, or draw scientific conclusions. All AI-assisted edits were reviewed and approved by the authors, who take full responsibility for the content of the manuscript.

3. Results

3.1. Effects of PN and PN-Derived Components on HFDPC Viability

To establish treatment conditions suitable for subsequent molecular analyses, we first evaluated the effects of PN on HFDPC viability. PN did not markedly reduce cell viability after 48 h of treatment across the tested dilution range (Figure 1A).

We next assessed the effects of five quantified PN-derived constituents, including D-pinitol, shikimic acid, catechol, hydroquinone, and 3-hydroxybenzoic acid, as well as a mixture of these five compounds. None of the individual compounds or the five-component mixture markedly reduced HFDPC viability after 48 h of exposure, although a concentration-dependent decrease in MTT signal was observed at higher concentrations (Figure 1B).

Based on these findings, treatment conditions without marked effects on cell viability were selected for subsequent gene expression analyses, as described in Section 2.3 and Supplementary Table S1.

3.2. PN and Its Components Modulate Follicle-Related Gene Expression in HFDPCs

We next examined the effects of PN on the expression of *ALPL*, *CTNNB1*, and *FGF1*, which were selected as representative genes associated with dermal papilla characteristics, Wnt/β-catenin signaling, and follicular growth regulation, respectively. PN treatment significantly increased the expression of all three genes at dilutions of 1/2000 and 1/500 after 48 h of exposure (Figure 2A).

We then examined whether individual PN-derived components reproduced aspects of the transcriptional response observed with the complete extract. *CTNNB1* expression was significantly increased by catechol at both tested concentrations, hydroquinone and

3-hydroxybenzoic acid at the lower concentrations, shikimic acid and D-pinitol at both concentrations, and the five-component mixture at both PN-equivalent concentrations.

For *ALPL*, significant increases were observed with catechol at the lower concentration, hydroquinone at both concentrations, and the five-component mixture at the 1/2000-equivalent concentration. Shikimic acid did not significantly alter *ALPL* expression, whereas D-pinitol significantly decreased its expression.

FGF1 expression was significantly increased by catechol, hydroquinone, 3-hydroxybenzoic acid, shikimic acid, and D-pinitol at both tested concentrations, as well as by the five-component mixture at both PN-equivalent concentrations (Figure 2B).

Overall, the individual constituents reproduced different subsets of the PN-associated transcriptional response, whereas the five-component mixture affected a broader combination of the three follicle-related genes examined.

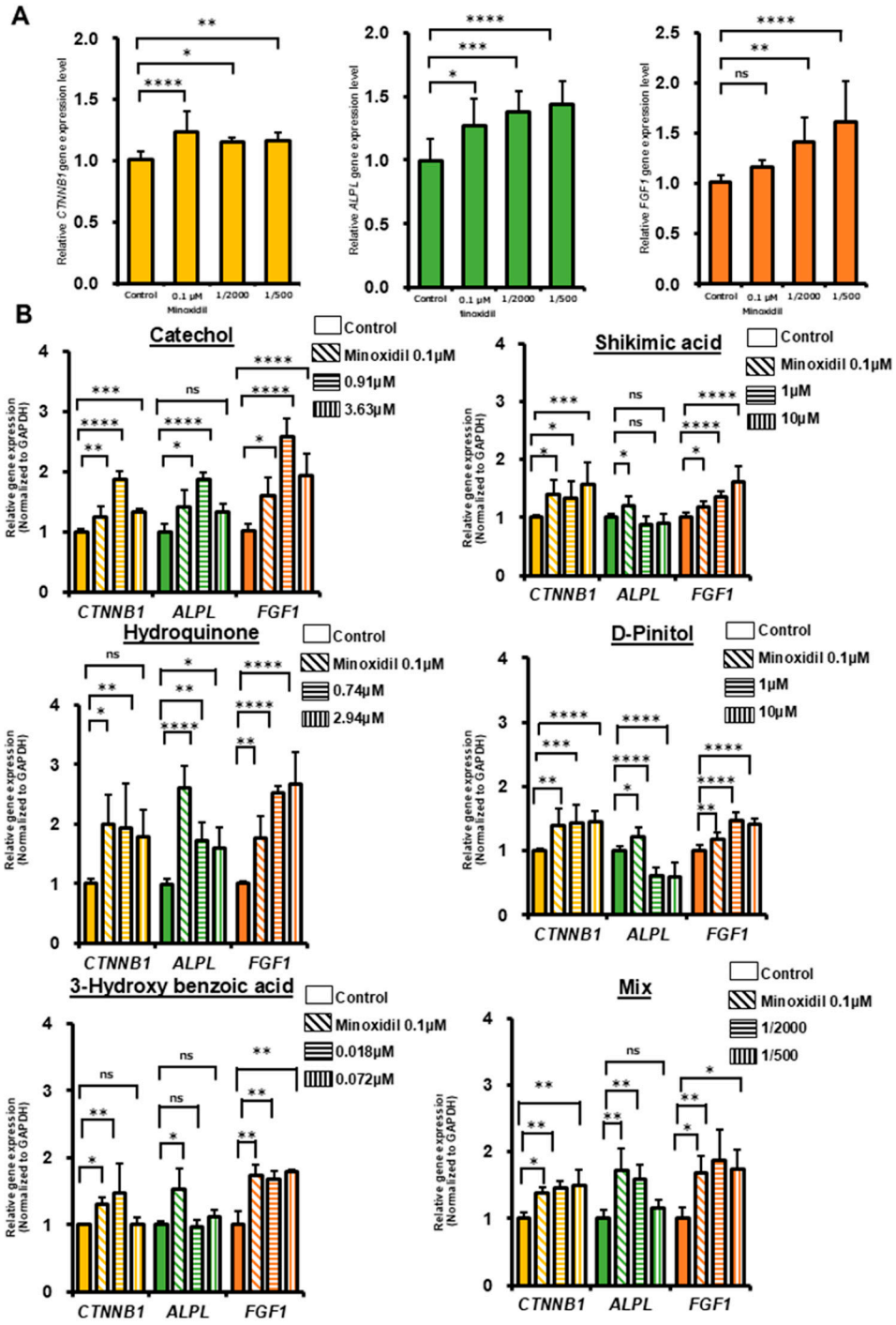

https://doi.org/10.3390/cosmetics13060331

Figure 2. Effects of PN and PN-derived components on follicle-related gene expression in HFDPCs. (**A**) HFDPCs were treated with the indicated dilutions of PN or with 0.1 μM minoxidil for 48 h, and the expression of *CTNNB1*, *ALPL*, and *FGF1* was measured by RT-qPCR. (**B**) HFDPCs were treated for 48 h with the indicated concentrations of PN-derived components or their mixture, and the expression of *CTNNB1*, *ALPL*, and *FGF1* was measured by RT-qPCR. Data are presented as mean ± SD from three independent experiments. Statistical significance was evaluated by one-way ANOVA followed by Dunnett's multiple-comparison test. For both panels, significance indicators are as follows: ns, not significant; * $p < 0.05$, ** $p < 0.01$, *** $p < 0.001$, and **** $p < 0.0001$ versus the control group.

3.3. Global Transcriptomic Changes Induced by PN in HFDPCs

To characterize the broader transcriptional response of HFDPCs to PN treatment, whole-genome microarray analysis was performed using the Clariom S Assay Human platform.

A total of 21,448 probe IDs were detected across all samples. The volcano plot illustrates the distribution of transcriptional changes between PN-treated and control HFDPCs, with significantly upregulated genes shown in red and significantly downregulated genes shown in blue (Figure 3A).

After application of the predefined quality filters and a statistical threshold of $p < 0.05$, 1336 PN-responsive genes were identified, including 667 upregulated and 669 downregulated genes (Figure 3B). Among these, *SLC6A2* showed the largest positive fold change (FC = 2.38), whereas *MX1* showed the largest negative fold change (FC = −3.66).

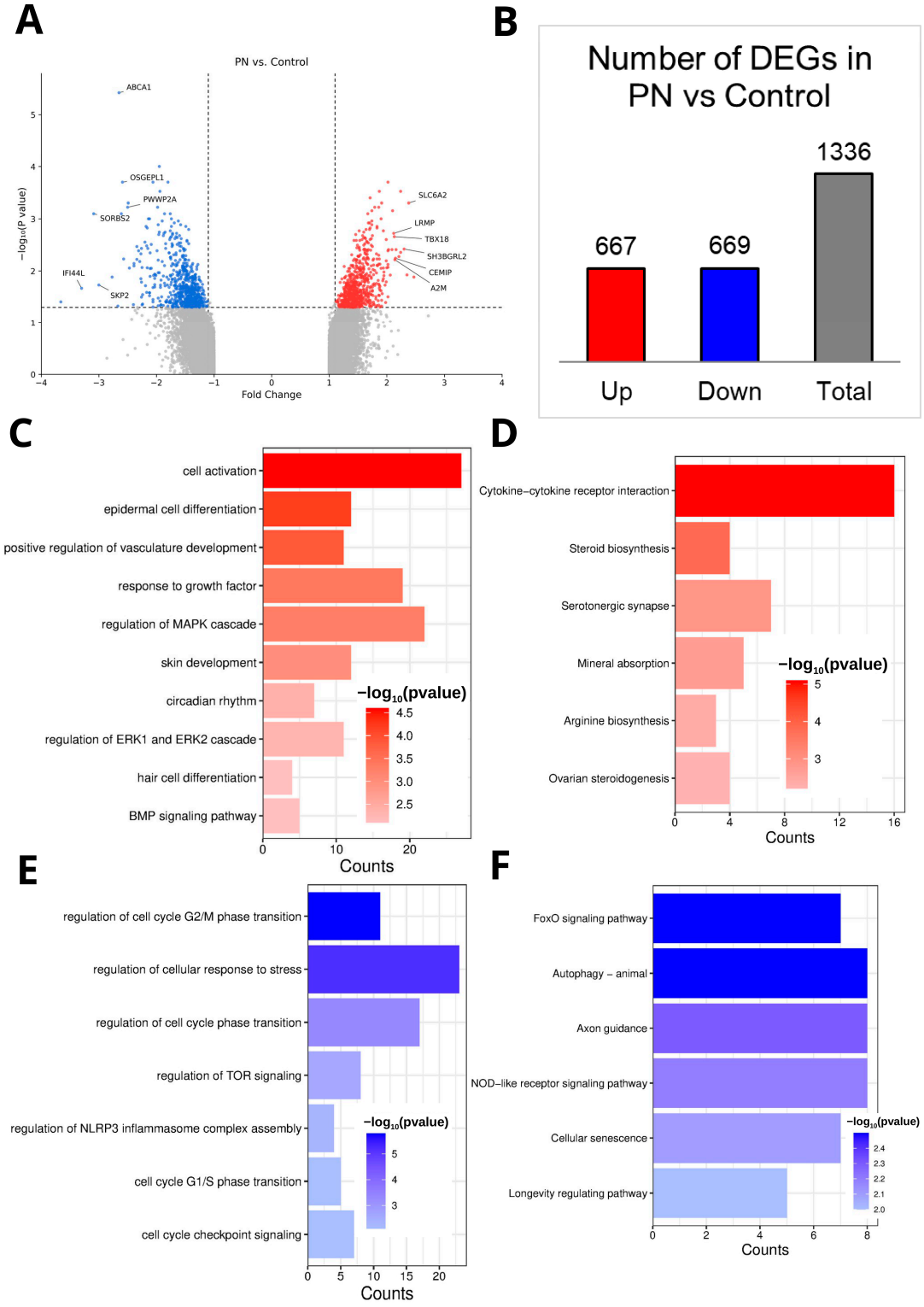

Figure 3. Transcriptomic response of HFDPCs to PN treatment. HFDPCs were treated with PN at a dilution of 1/500 for 48 h and analyzed by microarray. (**A**) Volcano plot of PN-responsive transcriptional changes in PN-treated versus control HFDPCs. The *x*-axis shows linear fold change, and the *y*-axis shows −log10(*p* value). Red dots indicate significantly upregulated genes, blue dots indicate significantly downregulated genes, and gray dots indicate genes that did not meet the statistical criterion. Representative genes with large fold changes are labeled. (**B**) Numbers of upregulated, downregulated, and total PN-responsive genes identified in PN-treated HFDPCs relative to controls. (**C**,**D**) Enrichment analysis of upregulated PN-responsive genes: (**C**) Gene Ontology (GO) biological

processes; (**D**) Kyoto Encyclopedia of Genes and Genomes (KEGG) pathways. (**E**,**F**) Enrichment analysis of downregulated PN-responsive genes: (**E**) GO biological processes; (**F**) KEGG pathways. In panels (**C**–**F**), bar color intensity indicates significance based on −log10(*p* value), and the *x*-axis indicates gene counts.

3.4. Functional Enrichment Analysis of PN-Responsive Genes in HFDPCs

To determine which biological processes and pathways were represented among the PN-responsive genes, GO and KEGG enrichment analyses were performed separately for the upregulated and downregulated PN-responsive genes.

GO biological process analysis of the upregulated genes identified enrichment of cell activation (GO:0001775), epidermal cell differentiation (GO:0009913), positive regulation of vasculature development (GO:1904018), response to growth factor (GO:0070848), regulation of the MAPK cascade (GO:0043408), skin development (GO:0043588), circadian rhythm (GO:0007623), regulation of ERK1 and ERK2 cascades (GO:0070372), hair cell differentiation (GO:0035315), and BMP signaling (GO:0030509) (Figure 3C).

KEGG analysis of the upregulated genes identified enrichment of cytokine–cytokine receptor interaction (hsa04060), steroid biosynthesis (hsa00100), serotonergic synapse (hsa04726), mineral absorption (hsa04978), arginine biosynthesis (hsa00220), and ovarian steroidogenesis (hsa04913) (Figure 3D).

In contrast, downregulated genes were enriched in GO biological processes related to regulation of the G2/M phase transition (GO:1902749), cellular response to stress (GO:0080135), regulation of cell-cycle phase transition (GO:1901987), TOR signaling (GO:0032006), regulation of NLRP3 inflammasome complex assembly (GO:1900225), G1/S phase transition (GO:0044843), and cell-cycle checkpoint signaling (GO:0000075) (Figure 3E).

KEGG analysis of the downregulated genes identified enrichment of FoxO signaling (hsa04068), autophagy—animal (hsa04140), axon guidance (hsa04360), NOD-like receptor signaling (hsa04621), cellular senescence (hsa04218), and longevity-regulating pathways (hsa04211) (Figure 3F).

Because the upregulated PN-responsive genes were enriched in multiple signaling pathways relevant to growth regulation and hair follicle biology, we next examined their functional connectivity using PPI-based pathway analysis.

3.5. PPI-Based KEGG Enrichment Analysis of Upregulated PN-Responsive Genes

To further characterize signaling relationships among the upregulated PN-responsive genes, a PPI network was constructed and subjected to KEGG pathway enrichment analysis.

The resulting PPI-derived network was enriched in pathways including ribosome, PI3K–Akt signaling, TNF signaling, neurotrophin signaling, autophagy—animal, EGFR tyrosine kinase inhibitor resistance, ErbB signaling, cell cycle, Ras signaling, insulin signaling, NF-κB signaling, VEGF signaling, longevity-regulating pathways, estrogen signaling, and Wnt signaling (Figure 4A).

Among these pathways, estrogen signaling was of particular interest because it was represented within the PN-responsive network and complemented the steroid biosynthesis and ovarian steroidogenesis signatures identified in the preceding enrichment analyses. We therefore examined estrogen-related network features in greater detail.

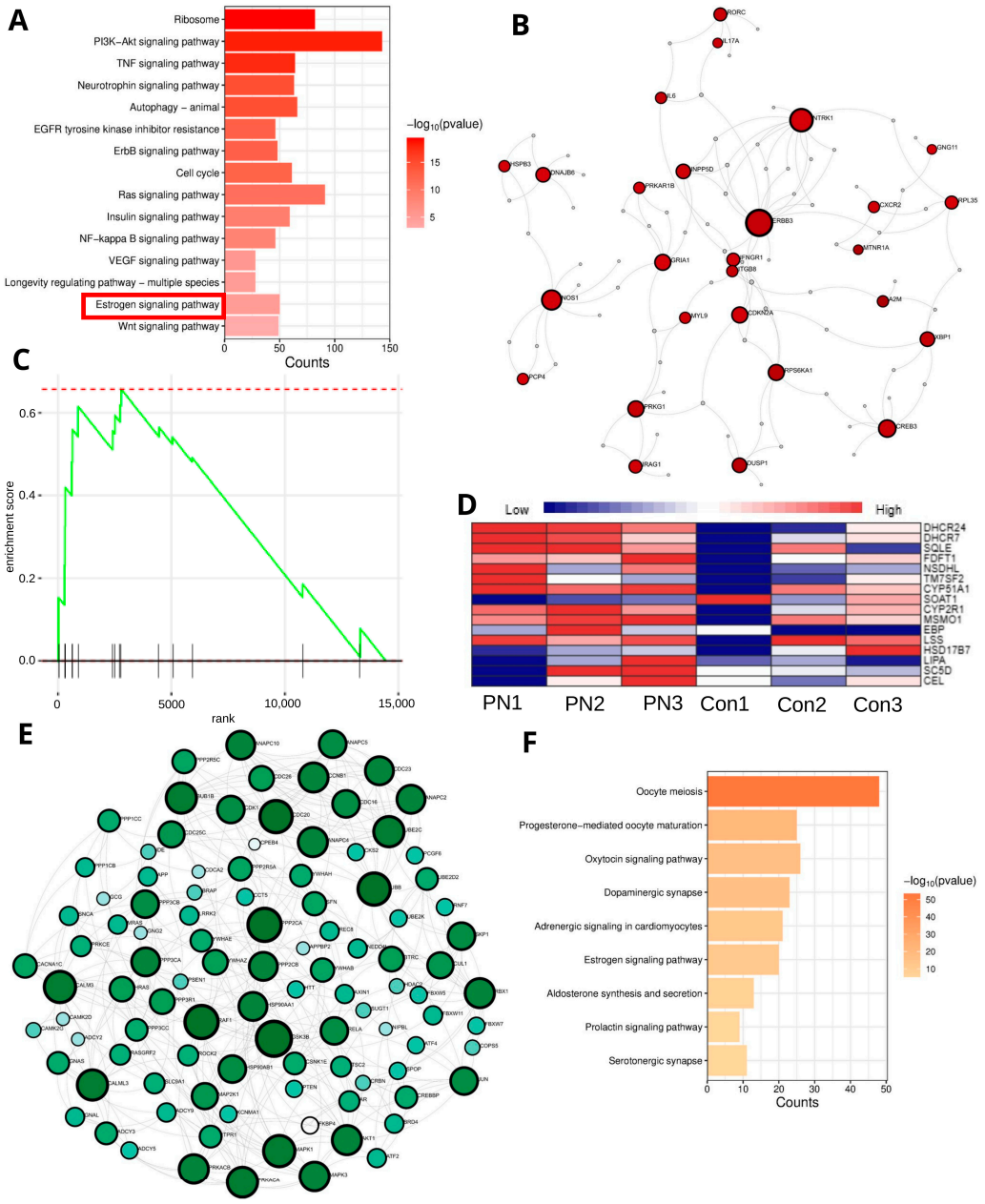

Figure 4. Network- and pathway-based analyses of estrogen- and sterol-related signaling in PN-treated HFDPCs and the comparative transcriptomic dataset. (**A**) KEGG pathway enrichment analysis based on the protein–protein interaction (PPI) network constructed from upregulated PN-responsive genes in PN-treated HFDPCs. The estrogen signaling pathway is highlighted by a red box to indicate its relevance to the present study and its further examination in panel B. (**B**) Estrogen-related subnetwork extracted from the PN-responsive PPI network. Red nodes indicate PN-responsive proteins included in the subnetwork, whereas gray nodes indicate connector nodes retained to preserve network structure. (**C**) Gene set enrichment analysis (GSEA) showing significant enrichment of steroid biosynthesis in PN-treated HFDPCs (enrichment score [ES] = 0.658, $p = 0.028$). (**D**) Expression-pattern heatmap associated with the KEGG steroid biosynthesis pathway identified by GSEA in three PN-treated and three control HFDPC samples. The heatmap was generated in ExpressAnalyst from SST-RMA-normalized expression data; no additional normalization was applied in ExpressAnalyst. (**E**) Oocyte meiosis-associated subnetwork extracted from the zero-order comparative PPI network generated from PN-responsive genes derived from the mouse hippocampal and HFDPC datasets. Node size reflects relative network connectivity. (**F**) KEGG pathway enrichment analysis of the oocyte meiosis-associated subnetwork, showing enrichment of hormone- and

neuroactive signaling pathways, including progesterone-mediated oocyte maturation, oxytocin signaling, dopaminergic synapse, adrenergic signaling, estrogen signaling, aldosterone synthesis and secretion, prolactin signaling, and serotonergic synapse.

3.6. Estrogen- and Sterol-Related Transcriptomic Features in PN-Treated HFDPCs

In total, 27 upregulated PN-responsive seed genes were represented in the estrogen-related PPI subnetwork (Figure 4B; Supplementary Table S3). These included ERBB3, NTRK1, NOS1, CREB3, PRKG1, and RPS6KA1 as prominent nodes. The network primarily represented genes associated with estrogen-related signaling and cellular responses rather than genes directly involved in estrogen biosynthesis.

Because steroid biosynthesis was also enriched among the upregulated PN-responsive genes, we next examined transcriptome-wide coordinated changes in sterol-related pathways using GSEA. Steroid biosynthesis was significantly enriched in PN-treated HFDPCs, with an enrichment score (ES) of 0.658 and $p = 0.028$ (Figure 4C).

A heatmap generated from three PN-treated and three control HFDPC samples further showed differential expression of genes involved in sterol biosynthesis-related processes, including *DHCR24*, *DHCR7*, *SQLE*, *FDFT1*, *NSDHL*, *TM7SF2*, *CYP51A1*, *CYP2R1*, *MSMO1*, *EBP*, *LSS*, *HSD17B7*, *LIPA*, *SC5D*, and *CEL* (Figure 4D).

Together, these analyses identified coordinated transcriptional changes involving estrogen-related signaling and sterol biosynthesis in PN-treated HFDPCs. These 27 PN-responsive genes represented in the estrogen-related PPI subnetwork were not individually validated by RT-qPCR.

3.7. Exploratory Comparative Transcriptomic Analysis Identifies Hormone-Related Network Features

To explore whether PN-responsive genes from distinct biological contexts showed convergence at the network level, we performed an exploratory comparison with our previously published mouse hippocampal transcriptomic dataset [12]. The purpose of this analysis was not to infer a common tissue-specific mechanism, but to identify potentially shared pathway-level features associated with PN exposure.

The HFDPC and mouse hippocampal datasets were analyzed independently, after which PN-responsive genes were integrated for zero-order PPI analysis in NetworkAnalyst. KEGG-based functional exploration identified an oocyte meiosis-associated subnetwork containing highly connected genes including *GSK3B*, *PPP2CA*, *RAF1*, *UBB*, *CDC20*, *CALM3*, *MAPK1*, *PRKACA*, *AKT1*, and *CDK1* (Figure 4E; Supplementary Table S2). Further enrichment analysis of this subnetwork identified several hormone- and neuroactive signaling pathways, including progesterone-mediated oocyte maturation, oxytocin signaling, dopaminergic synapse, adrenergic signaling, estrogen signaling, aldosterone synthesis and secretion, prolactin signaling, and serotonergic synapse (Figure 4F).

Because the datasets differed in species, tissue type, experimental model, exposure conditions, and microarray platform, these findings should be interpreted only as exploratory network-level similarities and not as evidence of a shared biological mechanism.

3.8. PN Increases ESR1 Expression in HFDPCs

Because estrogen-related signaling was represented in the PN-responsive pathway and network analyses, we independently examined whether PN affected the expression of *ESR1*, which encodes estrogen receptor alpha (ERα). In the microarray experiment performed with PN at 1/500 for 48 h, *ESR1* itself was not significantly altered (linear fold change = −1.20, $p = 0.0922$).

To examine *ESR1* expression under a separate targeted time-course condition, HFDPCs were treated with PN at 1/2000 and analyzed by RT-qPCR at 6, 12, and 24 h. No

significant difference in *ESR1* expression was observed at 6 h compared with the corresponding control. In contrast, *ESR1* expression was significantly increased at 12 h ($p < 0.01$) and remained significantly elevated at 24 h ($p < 0.05$) (Figure 5A).

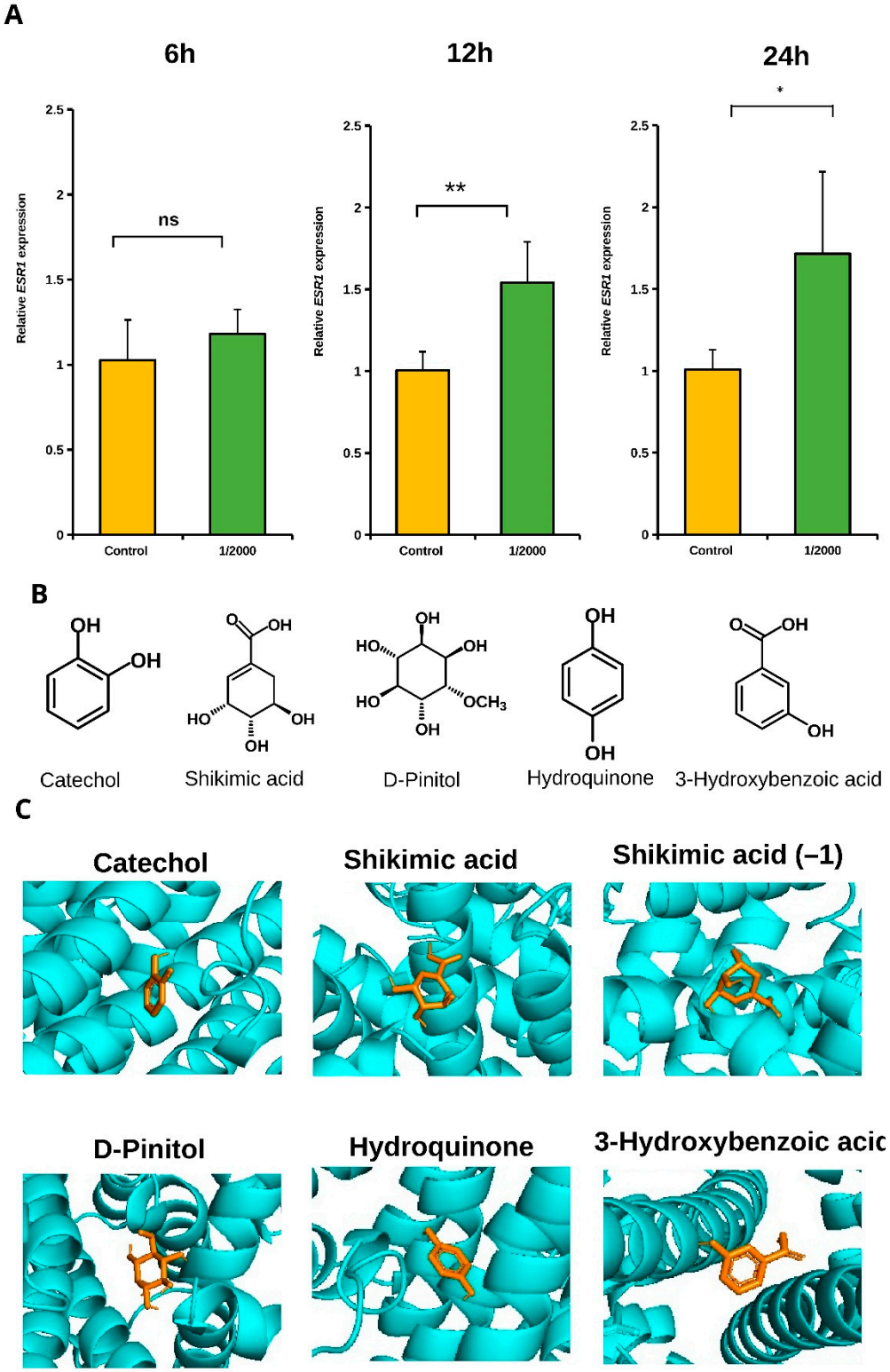

Figure 5. PN-induced *ESR1* expression and chemical structures and docking poses of PN-derived compounds. (**A**) HFDPCs were treated with PN at a dilution of 1/2000. *ESR1* mRNA expression was evaluated by RT-qPCR at 6, 12, and 24 h. PN-treated cells were compared with the corresponding control group at each time point using an unpaired Student's *t*-test. No significant difference was

observed at 6 h. *ESR1* expression was significantly increased at 12 h ($p < 0.01$) and remained significantly elevated at 24 h ($p < 0.05$). Data are presented as mean ± SD from three independent experiments. In panel (A), ns indicates not significant, * indicates $p < 0.05$, and ** indicates $p < 0.01$, compared with the corresponding control group at each time point. (**B**) Chemical structures of the five quantified PN-derived constituents examined in this study: catechol, shikimic acid, D-pinitol, hydroquinone, and 3-hydroxybenzoic acid. (**C**) Representative docking poses of PN-derived compounds in the ERα ligand-binding pocket. For shikimic acid, both the neutral form and the deprotonated form (−1 charge state) are shown. Docking simulations were performed using AutoDock Vina (version 1.2.7), and molecular structures were visualized using PyMOL (version 3.1.6.1).

These results indicate that PN increased *ESR1* expression under the 1/2000 time-course condition, although this response was not observed in the 1/500, 48 h microarray dataset.

3.9. Predicted Binding of PN-Derived Compounds to ERα

Because PN increased *ESR1* expression, we next examined whether selected PN-derived compounds were predicted to interact directly with ERα. The chemical structures of the five quantified PN-derived constituents examined in this study—catechol, shikimic acid, D-pinitol, hydroquinone, and 3-hydroxybenzoic acid—are shown in Figure 5B. Molecular docking was performed using 17β-estradiol (E2) as a reference ligand. For shikimic acid, both the neutral and deprotonated (−1) forms were evaluated.

E2 showed a predicted binding affinity of −7.5 kcal/mol. Among the PN-derived compounds, catechol showed the strongest predicted affinity (−5.1 kcal/mol), whereas shikimic acid, D-pinitol, and 3-hydroxybenzoic acid showed predicted affinities ranging from −4.7 to −4.9 kcal/mol. Hydroquinone showed a predicted affinity of −4.6 kcal/mol (Table 1, Figure 5C).

Under the present docking conditions, all tested PN-derived compounds showed weaker predicted binding to ERα than E2. Thus, although PN increased *ESR1* expression, the docking results did not support strong direct interaction of the tested PN-derived compounds with ERα.

Table 1. Predicted binding affinities of PN-derived compounds and 17β-estradiol toward ERα.

Compound	Predicted Binding Affinity (kcal/mol)
E2	−7.5
Catechol	−5.1
Shikimic acid	−4.8
Deprotonated shikimic acid (−1)	−4.7
D-pinitol	−4.9
Hydroquinone	−4.6
3-Hydroxybenzoic acid	−4.8

Molecular docking simulations were performed using AutoDock Vina. Docking scores are shown in kcal/mol, with more negative values indicating higher predicted binding tendencies. E2 was included as a reference ligand. The values represent the top-ranked docking pose for each compound.

4. Discussion

In the present study, PN induced coordinated transcriptional changes in HFDPCs without markedly compromising cell viability. At the targeted gene level, PN significantly increased the expression of *ALPL*, *CTNNB1*, and *FGF1*, which are associated with dermal papilla characteristics, Wnt/β-catenin signaling, and follicular growth regulation, respectively [6–8]. Several PN-derived components reproduced subsets of these gene expression changes, whereas the five-component mixture affected a broader combination of the examined genes. These findings suggest that the transcriptional response to PN may reflect the combined contribution of multiple constituents rather than the action of a single dominant compound.

Whole-transcriptome analysis further revealed broad transcriptional remodeling in PN-treated HFDPCs. Functional enrichment analysis identified biological processes related to epidermal differentiation, growth factor response, MAPK/ERK regulation, and skin development, while PPI-based KEGG analysis highlighted pathways including PI3K–Akt, Ras, VEGF, Wnt, and estrogen signaling. PI3K–Akt signaling has been implicated in hair follicle regeneration, while Wnt/β-catenin and other interconnected signaling pathways are established regulators of hair follicle development and cycling [22–25]. The simultaneous representation of these pathways suggests that PN exposure influences multiple signaling programs relevant to dermal papilla and hair follicle biology rather than a single isolated pathway.

One of the most prominent transcriptomic features was the enrichment of steroid biosynthesis-related pathways. GSEA showed significant enrichment of steroid biosynthesis, and multiple genes involved in cholesterol and sterol metabolism, including *FDFT1*, *SQLE*, *LSS*, *DHCR7*, *DHCR24*, *EBP*, *HSD17B7*, and *SC5D*, exhibited coordinated expression changes. These genes encode enzymes involved in multiple steps of sterol and cholesterol biosynthesis [26,27]. Cholesterol metabolism and sterol homeostasis are increasingly recognized as relevant to skin and hair follicle biology [28], and disruption of sterol metabolism has been associated with impaired follicular function and inflammatory skin changes [29]. The coordinated regulation observed here therefore identifies sterol biosynthesis as a potentially important component of the PN-induced transcriptional response in HFDPCs.

Estrogen-related signaling was also consistently represented across several levels of analysis. Estrogen signaling was enriched in the PPI-derived network, an estrogen-related subnetwork contained multiple interconnected PN-responsive proteins, and PN significantly increased *ESR1* expression at 12 and 24 h. Human hair follicles are both targets and local sources of estrogen-related signaling, and estrogen receptors are expressed in several follicular compartments [13]. Estrogen signaling has been implicated in the regulation of hair follicle cycling and dermal papilla cell responses, although its effects depend on receptor subtype, tissue context, and hormonal environment. More recently, ERα-associated signaling has also been linked to hair-related molecular responses in cultured human dermal papilla cells [15]. In this context, the increase in *ESR1* expression observed after PN treatment is consistent with a broader estrogen-related transcriptional response in HFDPCs.

Molecular docking was performed to examine whether major PN-derived compounds might directly interact with ERα. All tested compounds showed weaker predicted binding than 17β-estradiol, with catechol displaying the strongest predicted affinity among the PN-derived constituents. Thus, the observed increase in *ESR1* expression was not accompanied by docking evidence for strong direct ERα binding by the major compounds tested. These findings suggest that the estrogen-related transcriptional response to PN cannot be explained simply by high-affinity interaction of these constituents with the canonical ERα ligand-binding pocket.

The concurrent modulation of *CTNNB1* and *ESR1*, together with enrichment of both Wnt- and estrogen-related pathways, also raises the possibility of coordinated regulation between these signaling systems. Wnt/β-catenin signaling is a central regulator of hair follicle development and cycling [6], and interactions between estrogen receptor pathways and Wnt/β-catenin signaling have been described in other biological contexts [30]. Hair-related studies have also reported associations between estrogen-responsive signaling and Wnt/Hedgehog-related processes [14]. Although the present study does not establish direct pathway crosstalk, the parallel transcriptional changes suggest that Wnt- and estrogen-related signaling may form part of the broader molecular response of HFDPCs to PN.

The downregulated transcriptomic signatures provide an additional dimension to the PN response. GO and KEGG enrichment analyses identified processes related to cellular stress responses, TOR signaling, NLRP3 inflammasome regulation, cellular senescence, and longevity-associated pathways. Oxidative stress and inflammatory imbalance are known to influence the follicular microenvironment and hair follicle function [31]. Accordingly, the downregulated signatures may indicate that PN exposure also affects stress- and checkpoint-related transcriptional programs in HFDPCs, providing additional pathways for future mechanistic investigation.

The exploratory comparative analysis with the mouse hippocampal dataset provided a broader systems-level perspective. Integration of the two PN-responsive datasets identified an oocyte meiosis-associated subnetwork enriched in several hormone- and neuroactive signaling pathways, including estrogen, prolactin, oxytocin, dopaminergic, adrenergic, and serotonergic signaling. Highly connected genes such as *GSK3B*, *PPP2CA*, *MAPK1*, *PRKACA*, and *AKT1* participate in widely shared signaling processes. The recurrence of hormone-related network features across two distinct PN-responsive datasets suggests possible network-level convergence associated with PN exposure; however, the biological significance of this observation remains uncertain and the tissue-specific consequences are likely to differ substantially.

Several limitations define the scope of the present study. First, the experiments were performed in cultured HFDPCs and did not directly assess hair shaft elongation, hair follicle organ growth, or in vivo hair regrowth. Second, the sterol biosynthesis-related findings were derived from transcriptomic enrichment and gene expression patterns; cholesterol, sterol intermediates, and steroid hormones were not directly quantified. Third, molecular docking provides predicted binding poses and scores only and does not establish receptor activation. Fourth, protein-level validation and functional perturbation of estrogen- and Wnt-related pathways were not performed. Fifth, although the component experiments suggest that multiple constituents contribute to the PN-associated transcriptional response, the relative contribution and interaction of these constituents within the complete extract remain unresolved. Finally, the cross-tissue comparison should be regarded as hypothesis-generating. The HFDPC and mouse hippocampal datasets differed in species, tissue type, in vitro versus in vivo experimental context, PN exposure conditions, microarray platform, and statistical characteristics. The datasets were analyzed independently and integrated only at the ortholog-annotated gene/network level; expression values were not directly pooled. Consequently, platform-dependent dynamic range, study-specific variation, and potential batch effects cannot be excluded. The observed pathway-level similarities therefore do not establish a conserved PN mechanism across tissues and require validation in comparable experimental systems.

5. Conclusions

Pinus densiflora needle extract (PN) induced coordinated transcriptional changes in human hair follicle dermal papilla cells (HFDPCs), including increased expression of the

follicle-related genes *ALPL*, *CTNNB1*, and *FGF1* and broader modulation of Wnt-, growth factor-, estrogen-, and sterol biosynthesis-related pathways. PN also increased *ESR1* expression, whereas molecular docking indicated that the major PN-derived compounds tested showed weaker predicted ERα binding than 17β-estradiol. Together, these findings indicate that PN influences multiple transcriptional programs relevant to hair follicle biology, with prominent involvement of estrogen-related and sterol biosynthesis-associated signaling. Further functional studies, including biochemical sterol measurements, receptor- and protein-level validation, hair follicle organ culture, and in vivo models, will be required to determine the physiological significance of these transcriptional responses.

Supplementary Materials: The following supporting information can be downloaded at: https://www.mdpi.com/article/10.3390/cosmetics13060331/s1, Table S1. Concentrations of PN-derived compounds used in HFDPC gene expression experiments; Table S2. Representative hub genes in the oocyte meiosis-associated comparative PPI subnetwork; Table S3. PN-responsive upregulated genes represented in the estrogen-related PPI subnetwork in HFDPCs.

Author Contributions: Conceptualization, H.I.O., F.F., M.N., and H.I.; methodology, H.I.O. and H.I.; validation, H.I.O. and A.K.O.M.; formal analysis, H.I.O. and A.K.O.M.; investigation, H.I.O. and A.K.O.M.; resources, H.I.O. and H.I.; data curation, H.I.O. and A.K.O.M.; visualization, H.I.O.; funding acquisition, H.I.O., M.N., and H.I.; project administration, M.N. and H.I.; supervision, H.I.; writing—original draft preparation, H.I.O.; writing—review and editing, H.I.O., A.K.O.M., F.F., M.N., and H.I. All authors have read and agreed to the published version of the manuscript.

Funding: This work was partially supported by JST Grant Number JPMJPF2017. This research was also supported by Arakawa Chemical Industries, Ltd. through a collaborative research agreement with MED R&D Co., Ltd.

Institutional Review Board Statement: Not applicable. Commercially available human hair follicle dermal papilla cells were used in this study.

Informed Consent Statement: Not applicable.

Data Availability Statement: The HFDPC microarray data generated in the present study have been deposited in the NCBI Gene Expression Omnibus (GEO) under accession number GSE335947. The previously published mouse hippocampal microarray dataset used for the comparative transcriptomic analysis is available under accession number GSE293650.

Acknowledgments: Satellite AI was used solely for English-language polishing of the manuscript. It was not used to generate experimental data, perform statistical analyses, or draw scientific conclusions. All AI-assisted edits were reviewed and approved by the authors, who take full responsibility for the content of the manuscript.

Conflicts of Interest: Hisako Iwahashi Ogawa is employed by Arakawa Chemical Industries, Ltd., which funded this collaborative research and is involved in the commercialization of products containing *Pinus densiflora* needle extract (PN). Mitsutoshi Nakajima and Hiroko Isoda hold executive positions at MED R&D Co., Ltd., which received research funding from Arakawa Chemical Industries, Ltd. under a collaborative research agreement. MED R&D Co., Ltd. is not involved in the commercialization of PN-containing products. The remaining authors declare no conflicts of interest.

Abbreviations

3-HBA	3-hydroxybenzoic acid
5-HT	serotonin
Akt	protein kinase B
ALPL	alkaline phosphatase, biomineralization associated
ANOVA	analysis of variance

BMP	bone morphogenetic protein
BP	biological process
CTNNB1	catenin beta 1
DPCs	dermal papilla cells
E2	17β-estradiol
EBP	emopamil-binding protein
ERα	estrogen receptor alpha
ERβ	estrogen receptor beta
ERK	extracellular signal-regulated kinase
ES	enrichment score
ESR1	estrogen receptor 1
FBS	fetal bovine serum
FC	fold change
FGF1	fibroblast growth factor 1
GC/MS	gas chromatography–mass spectrometry
GO	Gene Ontology
GSEA	gene set enrichment analysis
HFDPCs	human hair follicle dermal papilla cells
HPLC	high-performance liquid chromatography
KEGG	Kyoto Encyclopedia of Genes and Genomes
LSS	lanosterol synthase
MAPK	mitogen-activated protein kinase
MTT	3-(4,5-dimethylthiazol-2-yl)-2,5-diphenyltetrazolium bromide
PPI	protein–protein interaction
PN	*Pinus densiflora* needle extract
ROS	reactive oxygen species
RT-qPCR	quantitative reverse transcription polymerase chain reaction
SD	standard deviation
SQLE	squalene epoxidase
TNF	tumor necrosis factor
VEGF	vascular endothelial growth factor
VEGFA	vascular endothelial growth factor A
Wnt	wingless/integrated

References

1. Moattari, C.R.; Jafferany, M. Psychological Aspects of Hair Disorders: Consideration for Dermatologists, Cosmetologists, Aesthetic, and Plastic Surgeons. *Ski. Appendage Disord.* **2022**, *8*, 186–194. https://doi.org/10.1159/000519817.
2. Jafferany, M. Trichopsychodermatology: The Psychiatric and Psychosocial Aspects of Hair Disorders. *Dermatol. Ther.* **2020**, *33*, e13168. https://doi.org/10.1111/dth.13168.
3. Asanad, K. Global Online Interest in Finasteride Sexual Side Effects. *Int. J. Impot. Res.* **2024**, *36*, 408–413. https://doi.org/10.1038/s41443-022-00612-1.
4. Bokhari, L. Sublingual Minoxidil for the Treatment of Male and Female Pattern Hair Loss: A Randomized, Double-blind, Placebo-controlled, Phase 1B Clinical Trial. *J. Eur. Acad. Dermatol. Venereol.* **2022**, *36*, e62–e66. https://doi.org/10.1111/jdv.17623.
5. Bai, L.; Wang, Y.; Wang, K.; Chen, X.; Zhao, Y.; Liu, C.; Qu, X. Materiobiomodulated ROS Therapy for de Novo Hair Growth. *Adv. Mater.* **2024**, *36*, 2311459. https://doi.org/10.1002/adma.202311459.
6. Choi, B.Y. Targeting Wnt/β-Catenin Pathway for Developing Therapies for Hair Loss. *Int. J. Mol. Sci.* **2020**, *21*, 4915. https://doi.org/10.3390/ijms21144915.
7. Huang, Y.; Fu, X.-B.; Guo, D.-J.; Li, X.; Wang, X.-J.; Xiao, J.; Lin, B.-B.; Lin, Z.-L.; Cai, P.; Jiang, L.; et al. Fibroblast Growth Factors Stimulate Hair Growth through β-Catenin and Shh Expression in C57BL/6 Mice. *BioMed Res. Int.* **2015**, *2015*, 730139. https://doi.org/10.1155/2015/730139.
8. Iida, M.; Ihara, S.; Matsuzaki, T. Hair Cycle-Dependent Changes of Alkaline Phosphatase Activity in the Mesenchyme and Epithelium in Mouse Vibrissal Follicles. *Dev. Growth Differ.* **2007**, *49*, 185–195. https://doi.org/10.1111/j.1440-169X.2007.00907.x.

9. Kwak, C.S.; Moon, S.C.; Lee, M.S. Antioxidant, Antimutagenic, and Antitumor Effects of Pine Needles (*Pinus densiflora*). *Nutr. Cancer* **2006**, *56*, 162–171. https://doi.org/10.1207/s15327914nc5602_7.
10. Ha, T.K.Q.; Lee, B.W.; Nguyen, N.H.; Cho, H.M.; Venkatesan, T.; Doan, T.P.; Kim, E.; Oh, W.K. Antiviral Activities of Compounds Isolated from *Pinus densiflora* (Pine Tree) against the Influenza A Virus. *Biomolecules* **2020**, *10*, 711. https://doi.org/10.3390/biom10050711.
11. Park, J.; Lee, B.; Choi, H.; Kim, W.; Kim, H.-J.; Cheong, H. Antithrombosis Activity of Protocatechuic and Shikimic Acids from Functional Plant *Pinus densiflora* Sieb. et Zucc Needles. *J. Nat. Med.* **2016**, *70*, 492–501. https://doi.org/10.1007/s11418-015-0956-y.
12. Ogawa, I.H.; Yasaka, E.; Kondo, S.; Ferdousi, F.; Nakajima, M.; Isoda, H. Antidepressant-like and Neuroprotective Effects of Pine Needle Extracts: Evidence from Behavioral, Transcriptomic, and Biochemical Studies. *EXCLI J.* **2025**, *24*, 1372–1396. https://doi.org/10.17179/excli2025-8720.
13. Ohnemus, U.; Uenalan, M.; Inzunza, J.; Gustafsson, J.-A.; Paus, R. The Hair Follicle as an Estrogen Target and Source. *Endocr. Rev.* **2006**, *27*, 677–706. https://doi.org/10.1210/er.2006-0020.
14. Yamano, M.; Yamanaka, Y.; Nishikawa, S.; Masujima, Y.; Ohue-Kitano, R.; Kimura, I. The GPR30 Agonist G-1 Promotes Hair Growth via Wnt/Hedgehog Signaling in Mice. *Front. Pharmacol.* **2025**, *16*, 1570922. https://doi.org/10.3389/fphar.2025.1570922.
15. Rim, H.; Kim, J.; Joo, J.H.; Kim, S.H.; Choi, Y.-H.; Shin, J.Y.; Kwack, M.H.; Lee, S.Y.; Jun, S.-H.; Sung, Y.K.; et al. Ferulic Acid Promotes Hair Growth via Estrogen Receptor Alpha Activation in Cultured Human Dermal Papilla Cells. *Sci. Rep.* **2026**, *16*, 8753. https://doi.org/10.1038/s41598-026-36774-x.
16. Hunter, J.D. Matplotlib: A 2D Graphics Environment. Comput. Sci. Eng. 2007, 9, 90–95. https://doi.org/10.1109/MCSE.2007.55.
17. Zhou, Y.; Zhou, B.; Pache, L.; Chang, M.; Khodabakhshi, A.H.; Tanaseichuk, O.; Benner, C.; Chanda, S.K. Metascape Provides a Biologist-Oriented Resource for the Analysis of Systems-Level Datasets. *Nat. Commun.* **2019**, *10*, 1523. https://doi.org/10.1038/s41467-019-09234-6.
18. Zhou, G.; Soufan, O.; Ewald, J.; Hancock, R.E.W.; Basu, N.; Xia, J. NetworkAnalyst 3.0: A Visual Analytics Platform for Comprehensive Gene Expression Profiling and Meta-Analysis. *Nucleic Acids Res.* **2019**, *47*, W234–W241. https://doi.org/10.1093/nar/gkz240.
19. Breuer, K.; Foroushani, A.K.; Laird, M.R.; Chen, C.; Sribnaia, A.; Lo, R.; Winsor, G.L.; Hancock, R.E.W.; Brinkman, F.S.L.; Lynn, D.J. InnateDB: Systems Biology of Innate Immunity and beyond—Recent Updates and Continuing Curation. *Nucleic Acids Res.* **2013**, *41*, D1228–D1233. https://doi.org/10.1093/nar/gks1147.
20. Liu, P.; Ewald, J.; Pang, Z.; Legrand, E.; Jeon, Y.S.; Sangiovanni, J.; Hacariz, O.; Zhou, G.; Head, J.A.; Basu, N.; et al. ExpressAnalyst: A Unified Platform for RNA-Sequencing Analysis in Non-Model Species. *Nat. Commun.* **2023**, *14*, 2995. https://doi.org/10.1038/s41467-023-38785-y.
21. Irizarry, R.A.; Hobbs, B.; Collin, F.; Beazer-Barclay, Y.D.; Antonellis, K.J.; Scherf, U.; Speed, T.P. Exploration, Normalization, and Summaries of High Density Oligonucleotide Array Probe Level Data. *Biostatistics* **2003**, *4*, 249–264. https://doi.org/10.1093/biostatistics/4.2.249.
22. Chen, Y.; Fan, Z.; Wang, X.; Mo, M.; Zeng, S.B.; Xu, R.-H.; Wang, X.; Wu, Y. PI3K/Akt Signaling Pathway Is Essential for de Novo Hair Follicle Regeneration. *Stem Cell Res. Ther.* **2020**, *11*, 144. https://doi.org/10.1186/s13287-020-01650-6.
23. Houschyar, K.S.; Borrelli, M.R.; Tapking, C.; Popp, D.; Puladi, B.; Ooms, M.; Chelliah, M.P.; Rein, S.; Pförringer, D.; Thor, D.; et al. Molecular Mechanisms of Hair Growth and Regeneration: Current Understanding and Novel Paradigms. *Dermatology* 2020, 236, 271–280. https://doi.org/10.1159/000506155.
24. Lee, S.B.; Lee, J.W.; Lee, H.; Lee, K.-J.; Hwang, H.W.; Shin, H.-T.; Byun, J.W.; Shin, J.; Choi, G.S. Dickkopf-Related Protein 2 Promotes Hair Growth by Upregulating the Wnt/β-Catenin Signaling Pathway in Human Dermal Papilla Cells. *Ann. Dermatol.* **2024**, *36*, 292–299. https://doi.org/10.5021/ad.23.128.
25. Lin, X.; Zhu, L.; He, J. Morphogenesis, Growth Cycle and Molecular Regulation of Hair Follicles. *Front. Cell Dev. Biol.* **2022**, *10*, 899095. https://doi.org/10.3389/fcell.2022.899095.
26. Ershov, P.; Kaluzhskiy, L.; Mezentsev, Y.; Yablokov, E.; Gnedenko, O.; Ivanov, A. Enzymes in the Cholesterol Synthesis Pathway: Interactomics in the Cancer Context. *Biomedicines* **2021**, *9*, 895. https://doi.org/10.3390/biomedicines9080895.
27. Qian, L.; Scott, N.A.; Capell-Hattam, I.M.; Draper, E.A.; Fenton, N.M.; Luu, W.; Sharpe, L.J.; Brown, A.J. Cholesterol Synthesis Enzyme SC4MOL Is Fine-Tuned by Sterols and Targeted for Degradation by the E3 Ligase MARCHF6. *J. Lipid Res.* **2023**, *64*, 100362. https://doi.org/10.1016/j.jlr.2023.100362.
28. Palmer, M.A.; Blakeborough, L.; Harries, M.; Haslam, I.S. Cholesterol Homeostasis: Links to Hair Follicle Biology and Hair Disorders. *Exp. Dermatol.* **2020**, *29*, 299–311. https://doi.org/10.1111/exd.13993.

29. Panicker, S.P.; Ganguly, T.; Consolo, M.; Price, V.; Mirmirani, P.; Honda, K.; Karnik, P. Sterol Intermediates of Cholesterol Biosynthesis Inhibit Hair Growth and Trigger an Innate Immune Response in Cicatricial Alopecia. *PLoS ONE* **2012**, *7*, e38449. https://doi.org/10.1371/journal.pone.0038449.
30. Wang, Y.; van der Zee, M.; Fodde, R.; Blok, L.J. Wnt/β-Catenin and Sex Hormone Signaling in Endometrial Homeostasis and Cancer. *Oncotarget* **2010**, *1*, 674–684. https://doi.org/10.18632/oncotarget.201.
31. Du, F.; Li, J.; Zhang, S.; Zeng, X.; Nie, J.; Li, Z. Oxidative Stress in Hair Follicle Development and Hair Growth: Signalling Pathways, Intervening Mechanisms and Potential of Natural Antioxidants. *J. Cell. Mol. Med.* **2024**, *28*, e18486. https://doi.org/10.1111/jcmm.18486.

Disclaimer/Publisher's Note: The statements, opinions and data contained in all publications are solely those of the individual author(s) and contributor(s) and not of MDPI and/or the editor(s). MDPI and/or the editor(s) disclaim responsibility for any injury to people or property resulting from any ideas, methods, instructions or products referred to in the content.